# Lattice Boltzmann simulation on continuously regenerating diesel filter

By Kazuhiro Yamamoto[1], Kazuki Yamauchi[1],
Naoki Takada[2], Masaki Misawa[2],
Hirohide Furutani[2], Osamu Shinozaki[2]

[1] *Department of Mechanical Science and Engineering, Nagoya University, Furo-cho, Chikusa-ku, Nagoya, Aichi 464-8603, Japan*
[2] *National Institute of Advanced Industrial Science and Technology (AIST), 1-2-1, Namiki, Tsukuba, Ibaraki 305-8564, Japan*

To reduce particulate matter (PM), including soot in diesel exhaust gas, a diesel particulate filter (DPF) has been developed. Since it is difficult to observe the phenomena in DPF experimentally, we have conducted a lattice Boltzmann simulation. In this study, we simulated the flow in a metallic filter. An X-ray computed tomography (CT) technique was applied to obtain its inner structure. The processes of soot deposition and oxidation were included for a continuously regenerating diesel filter. By comparing experimental data, a parameter of soot deposition probability in the numerical model was determined.

**Keywords: lattice Boltzmann method; X-ray CT; diesel exhaust gas; soot; DPF**

## 1. Introduction

Diesel vehicles, such as buses and trucks, are widely used in commerce. However, particulate matter (PM) contained in the diesel exhaust gas is considered to pose health risks and contribute to diseases and conditions, such as cancer and pollinosis [1,2]. Therefore, PM emission regulations have been markedly strengthened, particularly in Europe, North America, and Japan. For the after-treatment of diesel exhaust gas, the diesel particulate filter (DPF) has been developed to remove PM [3,4].

As a DPF removes PM, it will slowly become clogged with the PM it has adsorbed. This will cause the exhaust pressure to gradually increase and, consequently, fuel consumption will worsen. In the worst possible outcome, the diesel engine will stop working entirely. Therefore, when PM accumulates to some extent, it is necessary to replace the DPF with new one or to incinerate and remove the PM from the existing filter (filter regeneration) [5]. The future generation of this technology aims to develop a continuously regenerating DPF that continuously oxidizes adsorbed PM using a catalyst or a heater during operation of the vehicle. However, since the principle element of PM is carbon, the possibility exists that PM can spontaneously ignite under certain conditions, which causes cracking or erosion in the filter due to soot oxidation.

In order to solve these problems and to develop a filter that allows continuous regeneration, the processes of adsorption and oxidation of PM must be sufficiently

understood. In the development of existing filters, experiments primarily consist of injecting exhaust gas through filter samples and then estimating the amount of fine particles adsorbed inside the filter. In this scenario, usually, only the pressure difference across the filter and the temperature and composition of the exhaust gas can be measured. Therefore, a numerical simulation of the phenomena would be useful.

In the present study, a metallic fiber filter was analyzed to obtain its internal structure, using the X-ray CT method, and a numerical simulation was performed, using the obtained internal structure of the filter. We simulated a continuously regenerating DPF while simultaneously considering the deposition and combustion processes of soot particles.

## 2. Analytical model and X-ray CT measurement

In this section, a lattice Boltzmann method (LBM), used for the numerical model, is briefly explained [6,7]. The flow is described by the lattice BGK equation in terms of the distribution function. The evolution equation using the pressure distribution function is

$$p_\alpha(\boldsymbol{x}+\boldsymbol{c}_\alpha\delta_t, t+\delta_t) - p_\alpha(\boldsymbol{x},t) = -\frac{1}{\tau}[p_\alpha(\boldsymbol{x},t) - p_\alpha^{eq}(\boldsymbol{x},t)] \tag{2.1}$$

where $c = \delta_x/\delta_t$ and $\delta_x$ and $\delta_t$ are the lattice constant and the time step, and $\tau$ is the relaxation time that controls the rate of approach to equilibrium. The equilibrium distribution function, $p_\alpha^{eq}$, is given by

$$p_\alpha^{eq} = w_\alpha \left\{ p + p_0 \left[ 3\frac{(\boldsymbol{c}_\alpha\cdot\boldsymbol{u})}{c^2} + \frac{9}{2}\frac{(\boldsymbol{c}_\alpha\cdot\boldsymbol{u})^2}{c^4} - \frac{3}{2}\frac{\boldsymbol{u}\cdot\boldsymbol{u}}{c^2} \right] \right\} \tag{2.2}$$

The sound speed, $c_s$, is $c/\sqrt{3}$ with $p_0 = \rho_0 R T_0 = \rho_0 {c_s}^2$. Here, $p_0$ and $\rho_0$ are the pressure and density in the reference conditions. The pressure and local velocity of $\boldsymbol{u}(=(u_x,u_y,u_z))$ are obtained using the ideal gas equation.

$$p = \sum_\alpha p_\alpha \tag{2.3}$$

$$\boldsymbol{u} = \frac{\rho_0}{\rho}\frac{1}{p_0}\sum_\alpha \boldsymbol{c}_\alpha p_\alpha = \frac{T_0}{T}\frac{1}{p_0}\sum_\alpha \boldsymbol{c}_\alpha p_\alpha \tag{2.4}$$

In this study, to consider the variable density, we adopted the low Mach number approximation [7]. To perform the three-dimensional calculation, a d3q15 model was applied.

To analyze the combustion field for soot oxidation, the distribution functions of temperature and chemical species are required, in addition to the above distribution function of pressure. Similar to the flow field, the scalar quantities of temperature, soot, or oxygen concentration are obtained using the distribution function corresponding to each scalar quantity. The relaxation time is related to transport

coefficients, such as kinetic viscosity, using $\nu = (2\tau - 1)/6c^2\delta t$. The LBM formula for temperature and concentration fields is

$$F_{s,\alpha}(\boldsymbol{x} + \boldsymbol{c}_\alpha \delta_t, t + \delta_t) - F_{s,\alpha}(\boldsymbol{x}, t) = -\frac{1}{\tau_s}[F_{s,\alpha}(\boldsymbol{x}, t) - F^{eq}_{s,\alpha}(\boldsymbol{x}, t)] + w_\alpha Q_s \quad (2.5)$$

where $s$ is the temperature, $T$, or the mass fraction of species, $Y_i$, and $Q_s$ is the source term, due to the chemical reaction [7]. The equilibrium distribution function, $F^{eq}_{s,\alpha}$, is given by

$$F^{eq}_{s,\alpha} = w_\alpha \cdot s \left\{ 1 + 3\frac{(\boldsymbol{c}_\alpha \cdot \boldsymbol{u})}{c^2} + \frac{9}{2}\frac{(\boldsymbol{c}_\alpha \cdot \boldsymbol{u})^2}{c^4} - \frac{3}{2}\frac{\boldsymbol{u}^2}{c^2} \right\} \quad (2.6)$$

The temperature and the mass fraction of species are determined by these distribution functions.

$$T = \sum_\alpha F_{T,\alpha} \quad (2.7)$$

$$Y_i = \sum_\alpha F_{Yi,\alpha} \quad (2.8)$$

In a continuously regenerating DPF, the following three processes are included: (1) soot is reacted with oxygen in its gas phase; (2) the unburned soot in the first process is deposited onto the filter surface; and (3) the deposited soot burns on the filter surface. The deposition process of soot particles is explained by the Brownian diffusion, interception, inertial impaction, and gravity [8]. When the actual size of PM is taken into consideration, the analysis must be performed on the nanometer-scale and, consequently, a large computational cost will be needed for the calculation. Therefore, it is impractical to consider the complex geometry of nano-sized soot particles. Instead, the soot concentration is monitored at the surface of the filter or the soot layer [9]. The mass fraction of the deposited soot is given by

$$Y_{C,surface}(\boldsymbol{x}, t + \delta_t) = \sum_\alpha F_{C,\alpha}(\boldsymbol{x}, t) \cdot P_D + Y_{C,surface}(\boldsymbol{x}, t) \quad (2.9)$$

where $Y_{C,surface}$ is the mass fraction of soot on the filter surface or the deposited soot layer at each time step. It should be noted that $P_D$ is the soot deposition probability. Soot at $P_D$ is deposited. Soot at (1-$P_D$) is not deposited and is bounced back into the flow. Exfoliation of the soot layer, due to the flow, is not taken into consideration. Expectedly, $Y_{C,surface}$ is increased when the soot, in its gas phase, accumulates on the filter surface. As the soot deposition continues, the soot concentration sometime becomes unity. When this limit is reached, the solid site is piled up. The deposited soot region is treated as a non-slip wall, which implies a dynamic change in the boundary condition for the fluid. In this way, the soot deposition layer grows. When a continuously regenerating DPF is simulated, both

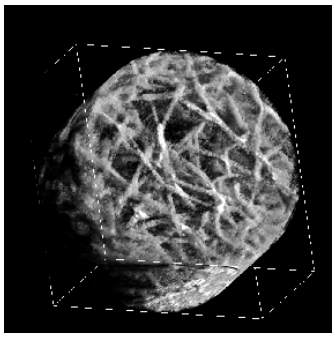

Figure 1. X-ray CT image of metallic filter.

the soot oxidation and the soot deposition are taken into consideration. In the present simulation, the soot oxidation was set as a one-step irreversible reaction, and a reaction rate proposed by Lee et al. was applied [10].

To analyze the flow inside an actual filter, the internal structure of the filter was obtained using a three-dimensional X-ray CT measurement [11]. Figure 1 shows the image of a filter obtained by this measurement. The image area was 6.65 mm $\times$ 6.65 mm $\times$ 3.46 mm, the pixel number in the cross section was 576 $\times$ 576, and the resolution in both horizontal (cross section) and vertical (deposition layer) directions was 11.5 $\mu$m/pixel. Based on projection data from the images, a three-dimensional matrix data of the filter with 576 $\times$ 576 $\times$ 300 points was obtained. The grid size in the simulation was the same value of the resolution in the CT measurement. The porosity of the filter is 0.8. The fiber structure of the filter is well observed.

## 3. Results and discussion

### (*a*) *Evaluation of soot deposition probability*

As mentioned above, the model was used to analyze the deposition phenomenon on the filter wall surface and the soot layer using the soot deposition probability, $P_D$. In this study, $P_D$ was experimentally evaluated. The experiment consisted of the following procedures. A 10 mm square of metallic fiber filter was cut out, using a diamond cutter, and the square was inserted into a sample holder with an 8 mm diameter hole. Exhaust gas from a diesel vehicle, whose mass concentration and PM particle-size distribution was already known [12], was flowed into the sample holder and the weight of the deposited PM onto the filter surface was measured. The mass of trapped soot inside the filter was counted using a Scanning Mobility Particle Sizer (SMPS), which was also evaluated by a CT image of the deposited soot inside the filter. The temperature of the filter was the same as that of the exhaust gas and the soot particles were deposited onto the filter without performing regeneration.

A field, consisting of the same conditions as the experiment, was reproduced as numerical calculations, and deposition calculations, with different values of $P_D$, were conducted. Just as occurred in the experiment, soot oxidation was not considered in the simulation and only soot deposition occurred. Figure 2 shows the time-variations of the amounts of soot deposited on the filter surface when $P_D = 0.0001$, 0.001, 0.01, 0.1, and 1.0. In figure 2, experimental data are indicated by the dotted

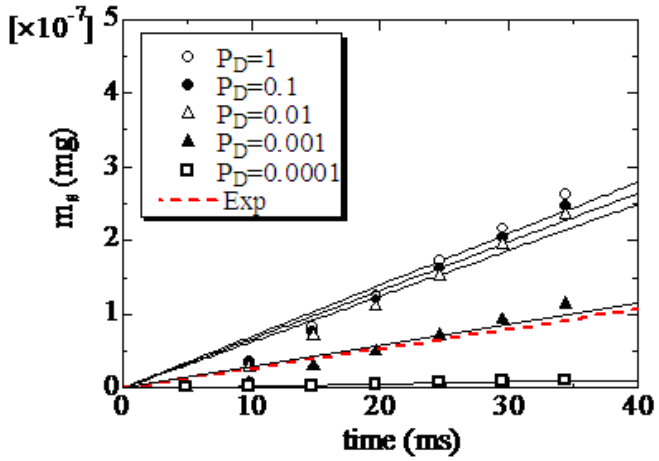


Figure 2. Mass of deposited soot in filter.

line. Furthermore, it can be seen that the amount of deposited soot was almost proportional to the passage of time. The amount of deposited soot increased with $P_D$. However, at $P_D > 0.01$, the total mass of deposited soot did not increase, because most of soot was trapped inside the filter. When the experimental results were compared with those obtained by the simulation, the temporal changes in the amount of deposited soot were close to the experimental values when $P_D = 0.001$. In the next section, a continuously regenerating DPF was simulated using $P_D = 0.001$.

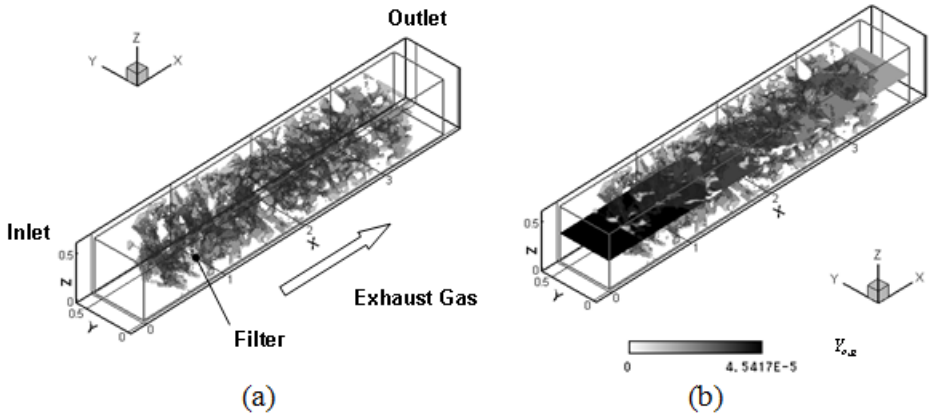


Figure 3. (a) Coordinate and calculation region, (b) soot in gas phase and deposited soot in solid phase; $t$=20ms, $T_w$=800°C.

### (*b*) *Simulation of a continuously regenerating DPF*

Figure 3 (a) shows the coordinate system and calculation domain used for the simulation. In the coordinate system, the direction of the exhaust gas flow passing through the filter is X, and the directions, perpendicular to the flow direction, are

Y and Z. The velocity components corresponding to these directions were expressed using $u$, $v$, and $w$, respectively. The size of the calculation domain was 3.695 mm in the X direction, and 0.589 mm in the Y and Z directions. The number of grid points was 320 (X) × 51 (Y) × 51 (Z). The filter was set at the center of the calculation domain, and entrance and exit zones were set in front of the filter region and at the rear of the filter region. Referring to the experiment, the conditions of the exhaust gas were set as follows: temperature, 400°C; mass fraction of soot, $4.54167 \times 10^{-5}$; and velocity, 0.497 m/s. The oxygen concentration of the exhaust gas and the filter temperature ($T_w$) were varied. Typically, the volumetric oxygen concentration of the exhaust gas was 10%.

Figure 3 (b) shows an example of the 3D profiles of soot at $T_w = 800$°C, which was obtained 20 ms after the initiation of the calculation. In figure 3 (b), the XY section expresses the distribution of the soot concentration in the gas phase, while the three-dimensionally displayed gray region expresses the solid phase of the deposited soot. As shown, the amount of soot in the exhaust gas decreased due to the soot deposition and combustion. Soot was primarily deposited onto a location near the inlet of the filter.

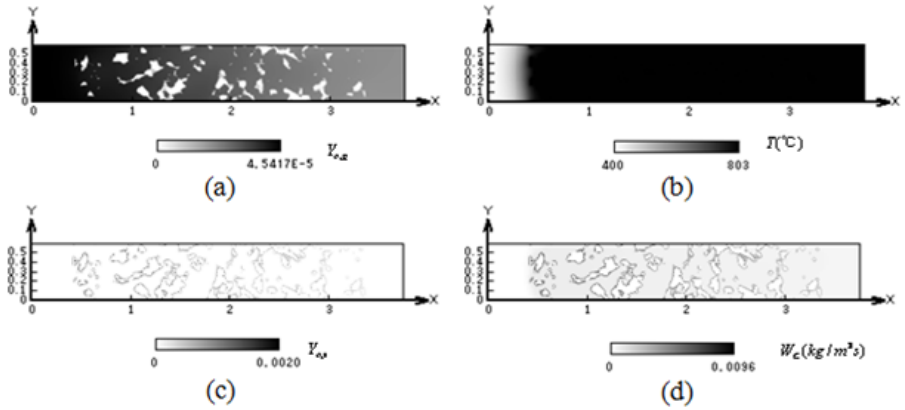


Figure 4. Distributions of (a) soot mass fraction in gas phase, (b) temperature, (c) accumulated soot mass fraction, (d) reaction rate; $t$=20ms, $T_w$=800°C.

Figure 4 shows the soot concentration in the gas phase ($Y_{c,g}$), the temperature ($T$), the concentration of deposited soot in the solid phase ($Y_{c,s}$), and the distribution of the reaction rate ($W_c$) on the XY section. As shown in the soot concentration in the gas phase, the soot concentration was not zero at the outlet of the filter. This means that the after-treatment of the filter was insufficient. For comparison, a calculation without considering soot deposition was performed. Consequently, the amount of burned soot was found to be very small at $T_w = 800$°C. Therefore, the decrease in the soot concentration was considered to be primarily due to soot deposition. The temperature distribution shown in figure 4 (b) indicates that the temperature increase, due to the soot combustion, was very small. The comparison between figures 4 (c) and (d) revealed that the reaction rate was particularly large on the filter surface. The reason for this is that, since the soot concentration increased with the soot deposition on the filter surface, the reaction rate increased on the filter surface. As mentioned above, when the filter tempera-

ture was 800°C, the after-treatment of the filter for the exhaust gas was insufficient and, consequently, unreacted soot, which had not been incinerated and removed, was emitted from the filter outlet.

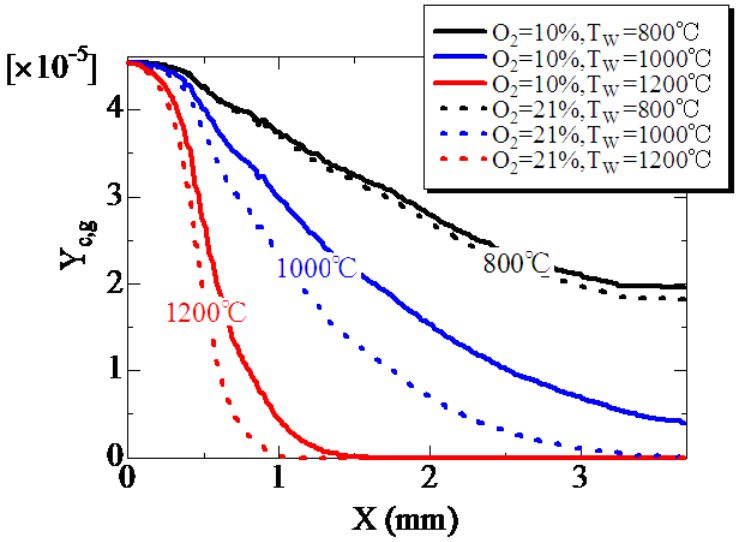


Figure 5. Soot mass fraction in gas phase; $t$=20ms.

Next, the effects of the filter temperature and oxygen concentration on the after-treatment of the exhaust gas were investigated, using different filter temperatures and oxygen concentrations. For quantitative investigation of the change in the soot concentration inside the filter, the soot concentrations in the gas phase on the YZ section were averaged, and the change in the soot concentration in the flow direction (X direction) was investigated. The filter temperature was set at 800°C, 1000°C, and 1200°C, and the volumetric oxygen concentration was set at 10% and 21%. Figure 5 shows the soot concentration distribution obtained when the soot concentration became stable 20 ms after the initiation of the calculation. As shown in figure 5, when the filter temperature was 800°C, independent of oxygen concentration, the soot concentration was not zero at the filter outlet; i.e., the after-treatment for the exhaust gas was insufficient. However, when the filter temperature was 1000°C or higher, soot in the exhaust gas was almost completely removed. When the oxygen concentration was higher, the decrease in the soot concentration in the exhaust gas was more substantial; i.e., the after-treatment for the exhaust gas was promoted. Based on these simulation results, it is possible to find the conditions of complete after-treatment in a continuously regenerating diesel filter.

## 4. Conclusion

In this study, using the internal structure of a metallic fiber filter obtained by an X-ray CT technique, the flow and reaction inside a diesel particulate filter were simulated using LBM. By simultaneously calculating soot deposition and oxidization processes, a continuously regenerating DPF was investigated. The following results were obtained:

(1) A comparison experiment showed that when the soot deposition probability of $P_D$ was 0.001, the time-variation of deposited soot in simulation significantly corresponded to the experimental data.

(2) Using the soot deposition probability evaluated by the experiments, a continuously regenerating DPF was simulated. Unburned soot in the gas phase was deposited onto the filter surface and, then, the deposited soot was oxidized.

(3) The amount of oxidized soot increased with the filter temperature. When the filter temperature was 1000°C or higher, soot in the exhaust gas could almost be completely eliminated in a continuously regenerating DPF.

(4) When the volumetric oxygen concentration was higher, soot was oxidized more significantly and, consequently, the after-treatment process in a continuously regenerating DPF was promoted.

## References

1. Hamada, H. & Obuchi, A. 2004 Recent trends; The after-treatment technologies of NOx and PM emission from diesel vehicles, *Engine Technology* **6**, 14–20.
2. Searles, R. A., Bosteels, D., Such, C. H., Nicol, A. J., Andersson, J. D., & Jemma, C. A. 2002 Investigation of the feasibility of achieving Euro V heavy-duty emissions limits with advanced emission control systems. In *Proc. FISITA 2002 World Automotive Congress, Helsinki, Finland, 2-7 June, 2002*, F02E310, pp.1–17.
3. Clerc, J. C. 1996 Catalytic diesel exhaust aftertreatment. *Appl. Catal. B-Environ.* **10**, 99–115.
4. Stratakis, G. A., Psarianos, D. L. & Stamatelos, A. M. 2002 Experimental investigation of the pressure drop in porous ceramic diesel particulate filters. *Proc. Inst. Mech. Eng. Part D-J. Automob. Eng.* **216**, 773–784.
5. Allensson, R., Blakeman, P. G., Cooper, B. J., Hess, H., Silcock, P. J. & Walker, A. P. 2002 Optimizing the low temperature performance and regeneration efficiency of the continuously regenerating diesel particulate filter (CR-DPF) system. In *Proc. SAE World Congress, Detroit, MI, USA, 4-7 March, 2002*, 2002-01-0428.
6. Yamamoto, K., Satake, S., Yamashita, H., Takada, N. & Misawa, M. 2007 Lattice Boltzmann simulation on flow with soot accumulation in diesel particulate filter. *Int. J. Mod. Phys. C* **18**, 528–535.
7. Yamamoto, K., Oohori, S., Yamashita, H. & Daido, S. 2009 Simulation on soot deposition and combustion in diesel particulate filter. *Proc. Combust. Inst.* **32**, 1965–1972.
8. Hinds, W. C. 1999 *Aerosol Technology*, 2nd edn., pp. 198. New York: John Wiley & Sons.
9. Yamamoto, K., Satake, S., Yamashita, H., Takada, N. & Misawa, M. 2009 Fluid simulation and X-ray CT images for soot deposition in a diesel filter. *Eur. Phys. J.-Spec. Top.* **48**, 205–212.
10. Lee, K. B., Thring, M. W. & Beer, J. M. 1962 On the rate of combustion of soot in a laminar soot flame. *Combust. Flame* **6**, 137–145.
11. Misawa, M., Tiseanu, I., Hirashima, R., Koizumi, K. & Ikeda, Y. 2004 Oblique view cone beam tomography for inspection of flat-shape objects. *Key Engineering Materials* **270**, 1135–1142.
12. Saito, K., Shinozaki, O., Yabe, A., Seto, T., Sakurai, H. & Ehara, K. 2008 Measuring mass emissions of diesel particulate matter by the DMA-APM method (First report) - Measurement of the effective density of diesel exhaust particles, *Review of Automotive Engineering* **29**, 83–90.